

DesignCon 2019

Baseline Wander: Systematic Approach to Rapid Simulation and Measurement

Pavel Zivny, Tektronix, 503-627-4755
pavel.zivny@tektronix.com

Vladimir Dmitriev-Zdorov, Mentor A Siemens Business
vladimir_dmitriev-zdorov@mentor.com, +1 720-494-1196

Maria Agoston, Tektronix,
maria.agoston@tektronix.com

I. Abstract

High speed serial data transmissions can suffer loss of margin as well as data errors due to baseline wander caused by mechanisms such as AC coupling. Thorough simulation and measurement are difficult since they involve interaction between physical layer fidelity features from sub-MHz to tens of GHz of signal spectra, and must include effects accumulated over millions of UIs.

We show a method of rapid analysis of baseline wander that quickly spans the large frequency range required, and consider its implementation in both bit-by-bit and statistical analysis. We demonstrate this method on extreme cases of signals in PAM4 signaling, and show measurement and simulation correlation.

II. Authors Biographies

Pavel Zivny

Pavel Zivny is a Domain Expert engineer with the sampling oscilloscopes group of Tektronix. He holds an MSEE degree and has been with Tektronix for over 20 years, working in test, design, and marketing of both real time and sampling oscilloscopes. Pavel was granted oscilloscope related patents, authored industry articles and papers, and represents Tektronix to high-speed Serial Data standards committees.

Vladimir Dmitriev-Zdorov

Dr. Vladimir Dmitriev-Zdorov is a principal engineer at Mentor, A Siemens Business. His work includes development of efficient methods of circuit/system simulation, transformation and analysis of multi-port systems, analysis of SERDES links. The results have been published in numerous papers and conference proceedings.

Maria Agoston

Maria Agoston is Principal Engineer with Tektronix. Her contributions to Tektronix instruments have been in the area of digital signal processing and jitter and noise analysis techniques. She holds a MS in Computer Engineering from Oregon State University and a MSEE from Polytechnic University of Bucharest. Maria has been awarded several patents in area of sampling oscilloscope waveform processing, and has authored several papers on high speed serial link analysis.

III. Introduction. What is Baseline Wander?

“Baseline wander is actually the effect where the base axis (X-axis) of any signal viewed on a screen appears to 'wander' or move up and down rather than be straight. ... I believe it is due to improper electrodes (like rusted, or broken)”

www.crazyengineers.com

*“...A long string 0s or 1s can cause a drift in the **baseline (baseline wandering)** and make it difficult for the receiver to decode correctly”*

<https://www.coursehero.com>

What is baseline wander (BLW)? Is this something caused by the lack of low frequency gain? Is it caused by having imbalance in symbols in the transmitted pattern? In fact, both conditions are necessary to cause BLW. It happens when channel has low frequency bandwidth limitations that block or significantly reduce part of the signal spectrum. The missing portion of the signal creates an error that manifests itself as a slow drift of the signal's median level. For example, PCIe channels include series decoupling capacitors. An unconstrained data stream travelling through such a channel would cause BLW, as an unconstrained signal can have a considerable amount of slowly changing data symbol imparity. To avoid BLW, the first generations of PCIe used data encoding protocols (8b10b) ensuring the signal pattern is DC-balanced. However, later generations employ less restrictive encoding to reduce encoding overhead and improve data transmission efficiency. They use scrambling that helps to distribute the energy of the signal evenly along frequency spectrum, thus reducing occasional low frequency spikes that occur in a raw un-encoded data stream. However, scrambling doesn't eliminate the low frequency portion of the signal spectrum completely, and hence – BLW remains a problem.

There are few works devoted to BLW in particular. However, the underlying phenomena were addressed over time in many sources on digital transmission, such as [1-3]. We can find there two major ways of mitigating BLW. One is using DC-balanced signal encoding protocols that prevent accumulation of signal disparity. The other is BLW correction through digital quantized feedback [4, 6]. Here, the missing BLW portion is “synthesized” on the receiver end by applying the restored digital signal to a low pass filter, and adding filtered waveform to the input of the receiver.

Both techniques have their limitations. DC-balanced protocols bear less net information per symbol than unconstrained patterns, and ever growing demand for speed forces the designers to trade BLW for efficiency. BLW correction is not widely used in modern high-speed communication. It is costly, and it's difficult to construct low pass filter that accurately approximates missing portion of the channel's transfer function.

Therefore, BLW noise remains an important factor that should be considered on the SERDES design and verification stage. Growing popularity of multilevel signaling (especially PAM-4) makes BLW impairment even more critical because of reduced separation between signal levels. Hence, we need accurate and efficient methods of BLW simulation and measurement.

BLW and current simulation tools

Unfortunately, BLW is not adequately addressed in existing analysis tools. Consider traditional bit-by-bit simulation of SERDES links, StatEye-type simulators, or IBIS AMI analysis, both time domain and statistical. Which of them consider impairments caused by

BLW? Most of the fast eye-diagram/BER evaluation methods are based on convolving a long digital stimulus with a relatively short channel's elementary response (impulse or step). For efficiency, they use overlap-save version of IFFT, but cannot afford a very long channel response (up to 1M symbols) that includes accurate near-DC bandwidth limitations. Even generating such response for statistical analysis is problematic. Similarly, new channel compliance evaluation methods, such as COM, ERL and others don't have provisions to consider effect of BLW. These approaches require that channel S-parameters be measured starting from 40-50MHz with a step of about 10MHz. With such sampling, the low frequency portion of the transfer function is completely ignored. The IFFT methods these tools employ require uniform sampling, and the computational cost of using ~10KHz steps going up to ~50GHz is prohibitive.

We can name only a few works evaluating BLW. In [5] the authors describe an approximate evaluation of BLW distribution, an important step in BLW analysis; [6] studies the effects of BLW on signal integrity for PCIe Gen 3 protocols, [7-8] investigate the effect of BLW on bit error ratio, and finds a short periodic test pattern that approximates its distribution.

Overall, there is no practically feasible systematic approach that can be used for BLW simulation and measurement. In this work, we propose a fast method of bit-by-bit simulation and a statistical BLW analysis. The latter assumes that the input pattern is either random and uncorrelated, correlated with known correlation function or spectral density, or is a deterministic periodic pattern. The method is majorly based on the idea of rational function approximation of the BLW transfer function, making it possible to avoid IFFT and use recursive convolution as a solution vehicle. Although is somewhat less convenient, it can also be used in a more traditional way, based on step/pulse responses. In either case, we need two convolution solvers, one for low-frequency BLW and the other for high-frequency ISI effects.

IV. Looking Deeper into BLW. Is it a Part of ISI or Something Else?

Despite the fact that phenomenon of baseline wander (BLW) has been known for years [2-7], it somehow remains a mystery, not sufficiently covered in literature or addressed in analysis tools. And yet, BLW is a serious factor: it produces slowly progressing low frequency noise that can reach several mV by magnitude, sometimes comparable or exceeding crosstalk. It affects bit error ratio, and is especially harmful for multilevel signaling protocols with smaller level separation.

We know that BLW appears in SERDES links which do not have a conductive connection between the signal transmitter and receiver, for example those using series DC-blocking capacitors or transformers. We also know that BLW is a relatively slow process that depends on both the channel's transfer function at low frequency, and the spectrum of the digital stimulus applied to the channel over considerable number of symbol intervals. In that respect, BLW is closely related to inter-symbol interference (ISI), as both are manifestations of the channel's bandwidth limitations. If so, why can't we consider BLW together with inter-symbol interference (ISI) and use similar techniques for their simulation and measurement? What is the difference between BLW and ISI?

To answer these questions, let's consider channels with bandwidth limitations at low frequency, high frequency, and both bandwidth boundaries. We understand that BLW is caused by low-frequency bandwidth deficiency (LFD), while ISI results typically from high-frequency bandwidth deficiency (HFD) or reflections. Figure 1 illustrates 3 cases: LFD, HFD, and both of them.

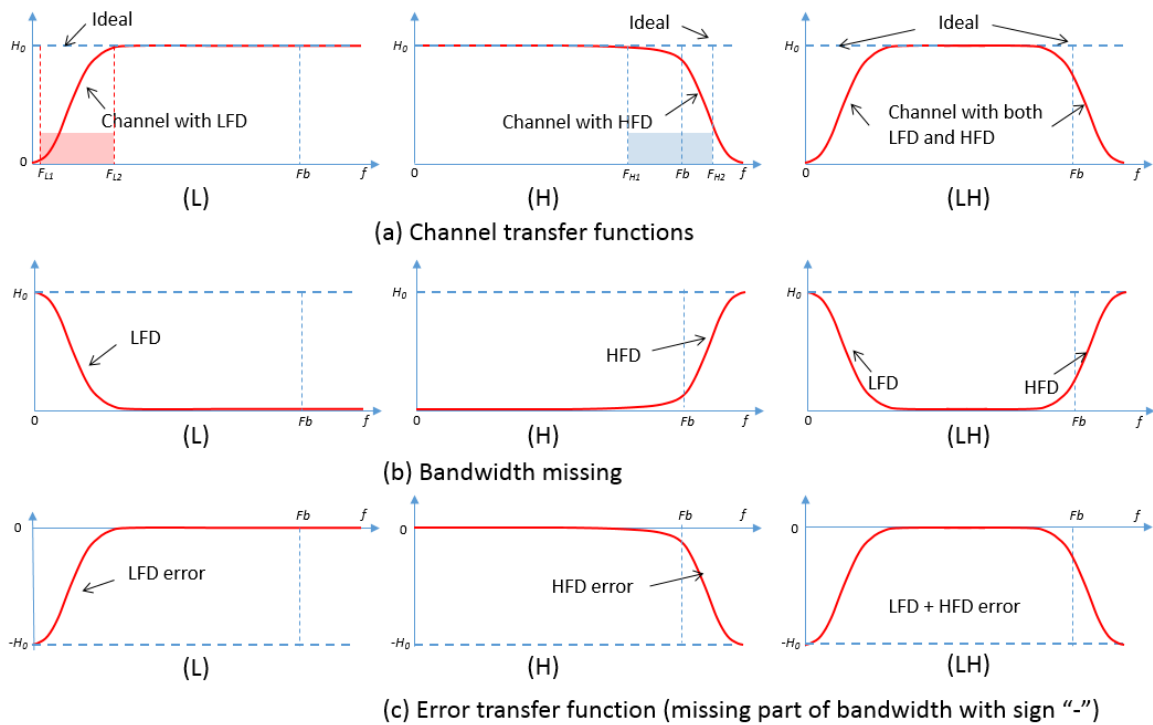


Figure 1. Channel transfer function (top row), missing bandwidth (middle), and error transfer function (bottom row). Left column corresponds to low-frequency deficiency, middle column – high-frequency bandwidth deficiency causing ISI, and right column has them both

Figure 1 illustrates channel transfer function with low- and high frequency limitations (top row). Middle row shows a missing portion of it, and bottom – an error transfer function. It is important to recognize the scale on frequency axis (which is far from being linear), and important frequencies and associated time constants. Let F_b be signal rate, and $T = 1 / F_b$ - symbol interval. In Figure 1(a, H) there is a band between frequencies F_{H1} and F_{H2} - marked blue - where most of the ISI effects reside. Typically, the length of the channel response needed for ISI estimation varies from a few hundred to a thousand of unit intervals, hence $F_b / F_{H1} \approx 100 \dots 1000$. Since we should allow several samples per UI, the waveform sampling rate, determined by F_{H2} , should be higher by an order or two: $F_{H2} / F_b \approx 10 \dots 100$. Low frequency bandwidth limitations span the range from F_{L1} to F_{L2} , Figure 1(a, L). This is a potential bandwidth of BLW error. Since F_{L2} defines the upper LFD limit, it is related to the time step that is small enough to capture all details of BLW noise. Typically, in channels with DC blocking capacitors F_{L2} doesn't exceed a few MHz, which is well below the signal rate $F_{L2} \ll F_b$. The lowest frequency of interest is F_{L1} ; this is where the channel's transfer function barely takes off. This frequency is in inverse proportion to LFD error response duration, or the time needed for BLW effect from a particular symbol to disappear. If we

assume exponential shape of LFD response, represented with $\sim 1\%$ accuracy, it would take about 400 uniform samples. However, it could be much larger with a more complicated frequency response, e.g. having low frequency resonances. Roughly, we can assume that $F_{L2} / F_{L1} \square 100 \dots 1000$.

As we see from above, low-frequency LFD-related noise has its own time scale, non-commensurable with simulation step and duration that we use for ISI. Sample interval for BLW noise doesn't have to be as small as for ISI. Depending on the ratio $F_b / F_{L2} \square 1$, even a symbol interval could be an unnecessarily fine granulation. If we have to simulate ISI together with BLW, it would take around a billion solution steps only to pass clear of a single BLW response duration. Therefore, it makes sense to separate computations of ISI and BLW and use individual time steps for both.

Figure 2 illustrates pulse responses of the channels with LFD and HFD separately, and combined. Its structure is similar to Figure 1. For convenience of drawing, the time constants related to ISI and BLW are made much closer to each other. A channel that doesn't modify the DC component of the input signal preserves the integral of the input pulse, which is $H_0 T$, see Figure 2, (a, H). The error, found as a difference between this pulse response and the ideal pulse is shown in Figure 2, (c, H). Integral over the error response is zero. Although ISI could be considerable, its accumulation doesn't create a slowly changing bias component.

On the contrary, for the channels with a non-transparent DC component (cases L and LH) the integral of the pulse response is zero, but not the integral on the error. The responses in the right column may look similar to those in the middle, but notice a small negative tail of the pulse response that stays long enough to zero-out the average. Respectively, the error component has a negative tail making the integral equal $-H_0 T$. Remarkably, this value doesn't depend on the low-frequency time constant, or exact shape of the channel response.

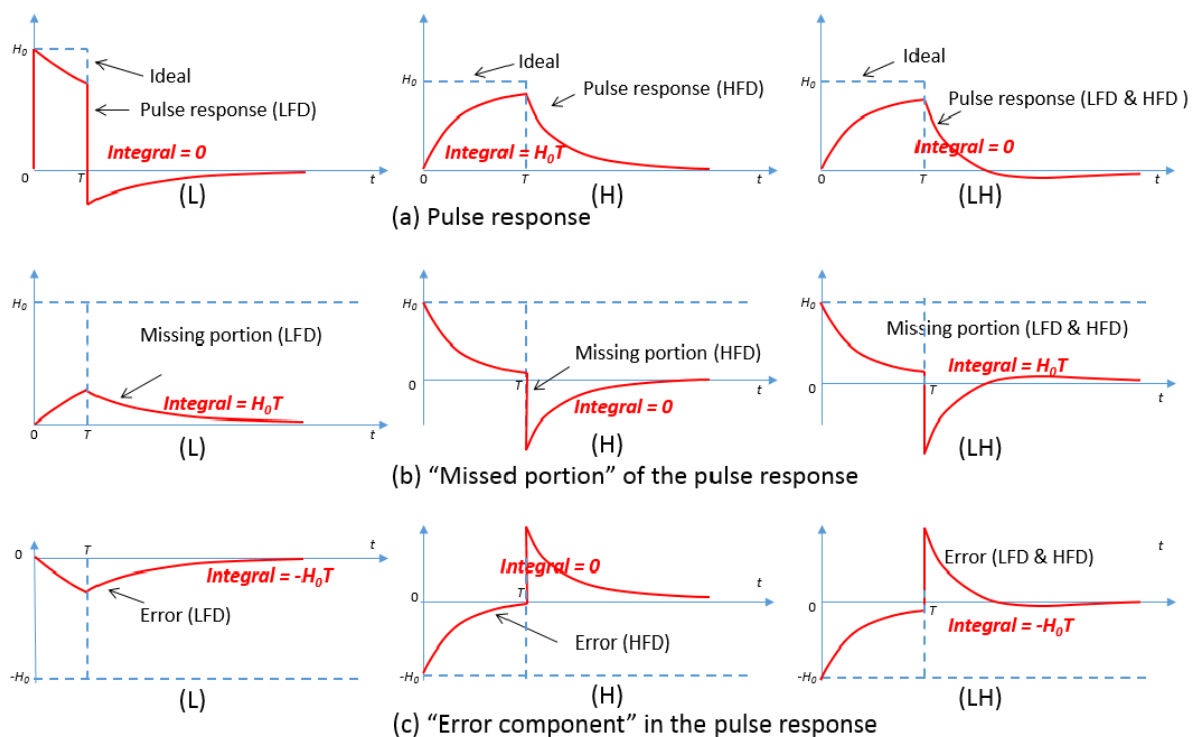


Figure 2. Pulse responses, characterizing the channels with LFD, HDF, and LDF & HFD. The structure is similar to Figure 1

What happens if we increase the value of the DC-blocking capacitor? The time constant of the error component, as in Figure 3 (c, L) will increase. Its peak value gets smaller, however its tail gets longer, as needed to preserve the value of the integral. As a result, BLW will be accumulated from increasingly many symbols, its behavior becomes less predictable and less correlated with the input pattern, at least within a time window we typically consider for ISI analysis. Even though the energy of the error coming from a single pulse remains constant, with more symbols involved, it's less probable that their magnitudes will be "biased" in concert, therefore the standard deviation of BLW decreases approximately as

$\sigma_{BLW} \approx H_0 \sigma_x \sqrt{\frac{T}{2\tau_{LF}}}$. Here, we assumed that input pattern is random uncorrelated, symbol amplitude has zero average and standard deviation σ_x ; T is symbol interval, H_0 - error transfer factor at DC, see Figure 1 (b, L), and τ_{LF} is a large time constant associated with error transfer function with response close to exponential.

A brief conclusion for this part:

- 1) Unlike ISI, BLW response is characterized by an error with a non-zero average. This explains its accumulation over time if the input pattern is not DC-balanced.
- 2) The duration of a BLW response is orders of magnitude longer than that for ISI effects, which makes it reasonable to compute them independently.
- 3) The, sampling interval needed to represent slowly changing BLW exceeds the symbol interval if $F_{L2} \ll F_b$. In this case it seems reasonable to aggregate several consecutive symbols together and use the "average" magnitude as an input to BLW filter.

V. Separating BLW transfer function from the full channel characteristic

In order to efficiently simulate BLW, we should separate its transfer function from the rest of the channel response. A proper way is to include the effect of linear equalization (FFE, CTLE) as well, but we won't consider it now because it doesn't modify the procedure described in this section.

One simple approach is first to find the characteristic by taking the samples on a coarse linear grid, as needed for accurate ISI representation. For example, if the channel characteristic from Figure 1 (a, LH) is sampled linearly with 10MHz spacing, starting from 50MHz, the low-frequency (BLW) portion will be completely ignored. Then, we can resample low frequency portion of the extracted response using a variety of interpolation methods (by Fourier transform, spline interpolation, rational fitting, etc.). This will give us characteristic behavior similar to Figure 1 (a, H). Then, we can find the characteristic of the same channel with much finer granulation going from DC up to 50MHz, or whatever frequency is needed to cover the effect from the blocking capacitor. The difference between the first characteristic (its LF portion) and the second gives us "BLW error transfer function", similar to the one shown in Figure 1 (b, L).

VI. Representing BLW transfer function by IIR filter

Since the BLW response duration may reach millions of UIs, time domain simulation methods using direct convolution (or its modifications, like overlap-save method) appear impractical. This group of methods belongs to finite-impulse-response filters (FIR). Instead, we'll use an infinite impulse response filter (IIR) by finding a rational approximation of the BLW transfer function [10, 11]. This approach is sufficiently accurate (max error below 0.1%), ensures causality, and allows fast recursive convolution, making it superior to direct convolution.

An arbitrary BLW transfer function can be represented as sum of elementary frequency components:

$$H(s) = H_\infty + \sum_{m=1}^M \frac{1}{2} \left[\frac{A_m}{1 + s / \Omega_m} + \frac{A_m^*}{1 + s / \Omega_m^*} \right]. \quad (1)$$

Here, M is the number of poles; A_m and Ω_m are real or complex factors and poles, with $\text{Re}\{\Omega_m\} > 0$. Then, for a given series of piece-wise constant (PWC) input - a sequence of digital symbols of magnitudes x_n - the output BLW becomes:

$$y(t_n) = H_\infty x_n + \text{Re} \sum_{m=1}^M z_{m,n}, \quad (2)$$

$$z_{m,n} = e^{-\Omega_m h_n} z_{m,n-1} + A_m [1 - e^{-\Omega_m h_n}] x_{n-1}. \quad (3)$$

Formulas (2, 3) give accurate solution in case of PWC input when the time points are taken at its nodes. These are modifications of PWL formulas such as those from [12]. Two simplifications are possible for BLW noise. First, its transfer function disappears at high frequency thus making $H_\infty = 0$. Second, PWC node points are evenly spaced, therefore we can set it to symbol interval $h_n = T$. Then (2, 3) become:

$$y_n = \sum_{m=1}^M \text{Re}\{K_m z_{m,n}\} \quad (4)$$

$$z_{m,n} = E_m z_{m,n-1} + x_{n-1}, \quad (5)$$

with constant complex factors $K_m = A_m(1 - e^{-\Omega_m T})$ and $E_m = e^{-\Omega_m T}$. Complex z_m are internal state variables; they should be updated once per solution point.

Expressions (4, 5) evaluate the output BLW error once per UI at the pinnacle of the pulse response and can be used as an efficient vehicle for time-domain BLW computations. We'll also use them to derive analytical form of the BLW noise pulse response - as in Figure 2 (c, L) - for statistical analysis.

VII. Representing BLW transfer function by FIR filter (direct convolution)

Once the channel response and BLW noise are separated in frequency, direct convolution methods employing FIR filtering become possible, too. For example, we can use step or pulse response representing BLW filter with much coarser time granulation compared to the signal response. With two separate responses, and two convolution engines (for BLW and ISI components) computations can be organized in a more efficient way.

In fact, there is a simple relation between IIR equations (4, 5) and BLW time response. The “cursors” of the BLW response on a single pulse, taken by symbol intervals, make a series

$$P_n = \sum_{m=1}^M \text{Re}\{K_m E_m^{n-1}\}, \quad n = 1 \dots N.$$

Of course, with direct convolution, the length of this series is always limited.

In this paper, we prefer using IIR filter described in the previous section. If necessary, it allows us to combine BLW and ISI effects together in a single filter. It also provides a convenient formal representation of responses, which we’ll use in the following sections.

VIII. Time domain analysis of BLW

Here we apply the techniques outlined in Section V and VI to the analysis of a FPGA design with 4uF series capacitors, operating at 5 Gbps. The wideband transfer function (TF) has been extracted from the design using a combination of logarithmic and linear spacing, spanning the range from 10Hz to 50 GHz. The BLW noise TF (Figure 3, blue curve) was found as a difference between the one with LF portion extrapolated down to DC (red curve), and the full broadband TF (green).

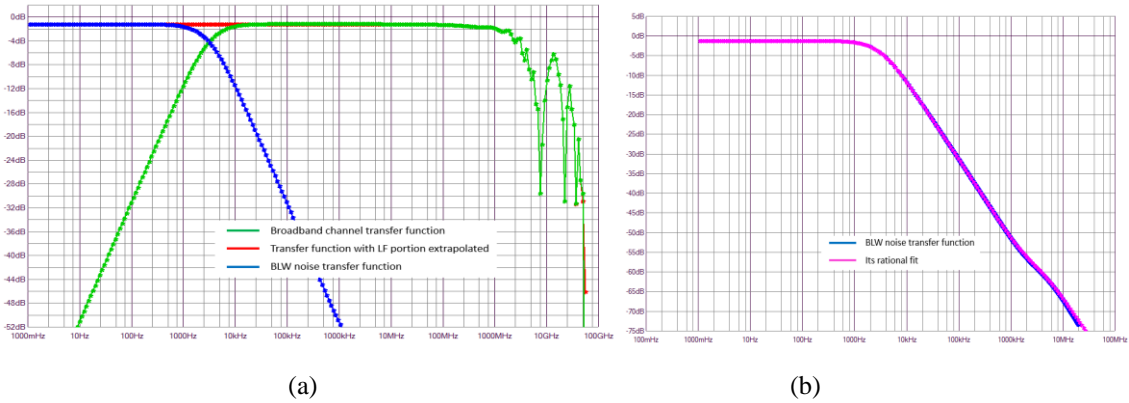


Figure 3. (a) Broadband transfer function, its version using flat continuation for the missing LF portion, and BLW noise transfer function, the difference between the two; (b) sampled transfer function of BLW and its fit

We used a non-periodic random unconstrained NRZ pattern with 5 Gbps. The BLW transfer function drops by 60dB at frequency that is about 3 orders of magnitude below the bit rate. The time constant of the BLW components is two more orders of magnitude below that, where the green and blue curves cross. Our expectation therefore is that BLW accumulates the effect from approximately 100K symbols, but is only sensitive to symbol imparity averaged over about 1,000 symbols and not to its faster variations.

The fitted version of the BLW function is represented by 7 real and complex poles. Poles and residues were used to construct an IIR filter, as defined by equations (4, 5). We performed a series of simulations updating state variables per equal time intervals. First, once per symbol, with x_n in (5) being actual symbol values (1, -1). Then, the state variables were updated every p symbols, with $p = 10, 100 \dots 100K$. For each group of p consecutive symbols we determined the average and used it as an “aggregated symbol” when updating state variables in (5).

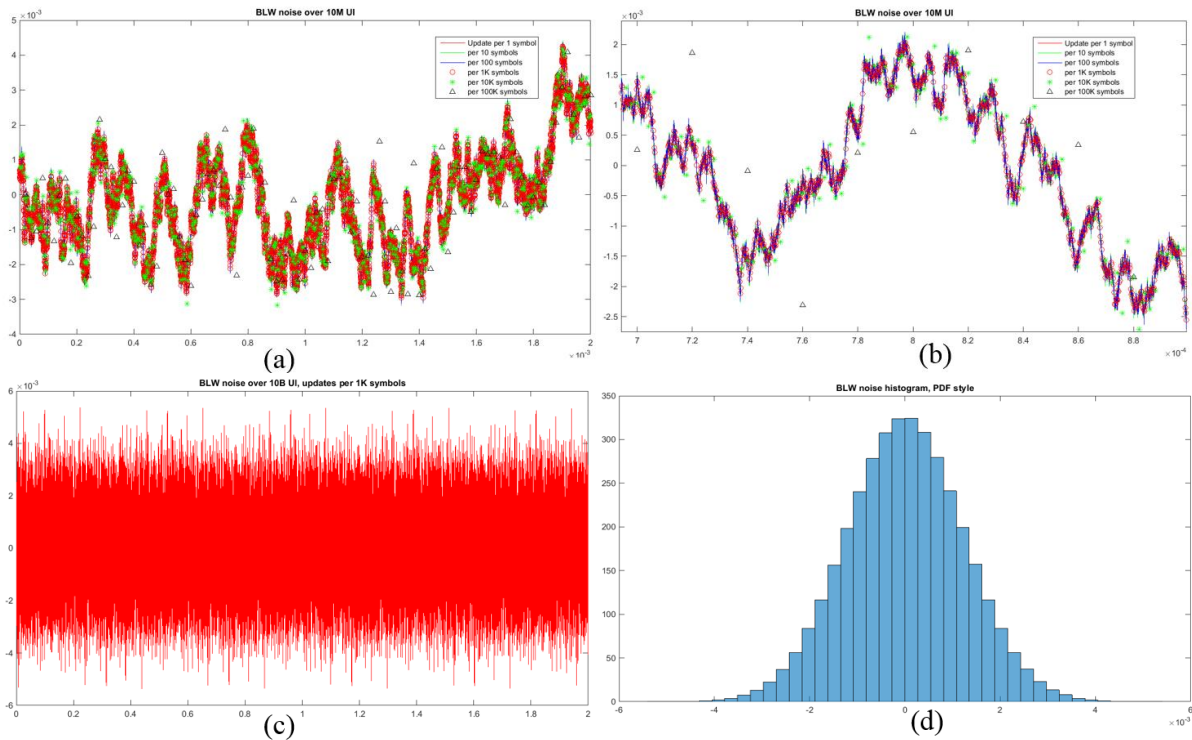


Figure 4. (a) BLW computed over 10M bits with different granularity; (b) same waveforms, zoomed; (c) BLW computed over 10B symbols with updates every 1K symbols; (d) BLW noise histogram build from 10B UI waveform

As we see from Figure 4 (a, b), only extremely rare updates, once per 10K (marked green star) or 100K (marked with triangles), differ from those found with finer granulation. This result agrees with our observations of frequency responses from Figure 3. We found that updating state variables once per 1K symbols provides high simulation accuracy of BLW, and is much faster than updating every symbol. Therefore, the next experiment comprises of computing BLW over 10B symbols with 1K symbol updates, going over 2 seconds of the “model time”. The resulted noise waveform and the histogram built from it are shown in Figure 4, (c) and (d).

This approach is indeed very fast. On a Dell M4800 it takes about 1 sec of CPU time per 100M symbols. In this example, that’s only about 70 times slower than real-life hardware operation.

It’s tempting to say that this fast time domain simulation of BLW provides a way to build distribution down to low probability levels. Let’s imagine that we have a fast solver that can simulate up to 10^{12} symbols in this manner, together with BLW noise. After we build the eye, can we say that BLW noise distribution was accounted down to $\approx 10^{-12}$ probability level? Unfortunately, the answer is “no”. As we mentioned before, BLW and ISI effects have quite different bandwidth limits. When we estimate histogram of a random process, only uncorrelated data samples are statistically meaningful. Since correlation interval of BLW process is about $\sim \tau_{LF} / T$ of UIs, we need to increase the time of BLW estimation in the same proportion. In our test example this ratio is 6 order of magnitudes! Whatever the time domain simulation speed is, we cannot hope to cover 10^{18} symbols.

That’s why statistical analysis of BLW is extremely important.

IX. Statistical analysis of BLW

Let's unwrap recursive convolution formulas (4, 5) and explicitly express the output BLW samples through symbol values. By applying (5) repeatedly for N consecutive symbols, we get the value of the m -th state variable:

$$z_{m,N} = E_m^{N-1}x_1 + E_m^{N-2}x_2 + \dots + E_mx_{N-1} + x_N. \quad (6)$$

Therefore, the output becomes $y_N = \text{Re} \sum_{m=1}^M K_m \sum_{n=1}^N E_m^{N-n} x_n$. By changing the order of

summation, we can write it as $y_N = \sum_{n=1}^N P_n x_n$, where $P_n = \sum_{m=1}^M \text{Re}\{K_m E_m^{N-n}\}$. For the purpose of

statistical analysis, we can assume that the property of the input pattern doesn't change with time inversion: it can be played backward and reveal the same statistical properties. If so, symbol values x_k can be replaced by x_{N-k+1} and the output values represented as:

$$y_N = \sum_{n=1}^N P_n x_n, \text{ where } P_n = \sum_{m=1}^M \text{Re}\{K_m E_m^{n-1}\}. \quad (7)$$

Random uncorrelated input pattern, even centered distribution

Let's assume that input symbols have L -level modulation (PAM- L), with all states equally probable, meaning they average to zero and are uncorrelated. Due to the considerable difference between the signal rate and BLW processes, the low-pass filter will efficiently average the effect from individual symbol over hundreds or thousands of bits, thus making the distribution of BLW noise close to Gaussian.

We'll estimate standard deviation of the output samples described by (7). A square of standard deviation of y_N is $\sigma_y^2 = \langle (y_N - \bar{y})^2 \rangle$. We assume that the mean value of a symbol magnitude is zero, thus making the mean value of the output zero, too. Therefore, we need to find an average of the product of the two sums:

$$\sigma_y^2 = \left\langle \left(\sum_{n=1}^N P_n x_n \right) \left(\sum_{q=1}^N P_q x_q \right) \right\rangle. \quad (8)$$

Note that since x_n are statistically independent, the average of the product $\langle x_n x_q \rangle$ is zero for all $n \neq q$. Therefore, (8) reduces to a sum of components with squared factors only:

$$\sigma_y^2 = \sum_{n=1}^N P_n^2 \langle x_n^2 \rangle = \sigma_x^2 \sum_{n=1}^N P_n^2. \quad (9)$$

Dispersion of the input symbols is defined by their largest magnitude A_s and the number of signal levels as

$$\sigma_x^2 = A_s^2 \frac{L+1}{3(L-1)}. \quad (10)$$

Hence the only remaining task is to find the sum in (9).

The summands in (9) don't form a geometrical progression, as we'd have for an exponential component; they may have components oscillating with different frequencies and attenuating

with different rate. Therefore, the sum (9) doesn't converge monotonically with N . However, since we know the slowest pole in approximation (1), we can easily estimate the number of summands that guarantees convergence with predefined accuracy. Let $\Omega_{\min} = \min \text{Re}\{\dot{\Omega}_m\}$. For a given error $\varepsilon \ll 1$, we can estimate the number of summand from $e^{-N\Omega_{\min}T} < \varepsilon$. In our case $\Omega_{\min} = 2\pi * 3.128e3$ therefore for $\varepsilon = 10^{-10}$ we should consider about 5.8M summands.

Figure 5 below, illustrates convergence of the sum while considering 10M summands. While the number seems large, the computations are simple and take about a second. As we see, the summands in (9) (red curve) start to decrease monotonically only for $N > 100K$, after the faster poles disappear. Their increments (green) are much smaller but follow the trend. The estimate of sigma – a square root of the current sum (shown black) doesn't visibly change after $N \geq 5e5$. However 15 digits of sigma estimate settle after about $N = 3.2M$ symbols.

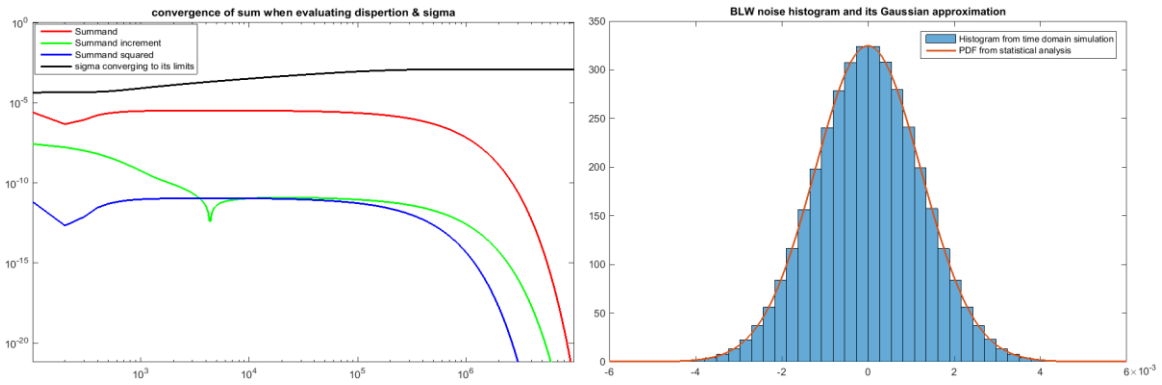


Figure 5 (a) convergence of the sum and BLW standard deviation; (b) comparison of BLW histogram found by 10B time-domain analysis and PDF predicted by statistical method

The resulting sigma is 1.228 mV, considering that for unit-magnitude NRZ $\sigma_x^2 = 1$. Found statistical distribution perfectly matches the histogram from 10B-symbol BLW simulation.

Correlated input pattern

What if the input symbols are not statistically independent? If so, they are correlated, and the average $\langle x_n x_{n+k} \rangle$ is not zero even for $k \neq 0$. In this case, finding the average of the expression (8) becomes more complicated. We assume that input pattern is a stationary process and its statistical properties don't change over time. Therefore, the average $C_{x,k} = \langle x_n x_{n+k} \rangle$, $C_{x,0} = \sigma_x^2$ could be non-zero but doesn't change with n . Then dispersion of BLW becomes:

$$\sigma_y^2 = \left\langle \left(\sum_{n=1}^N P_n x_n \right) \left(\sum_{q=1}^N P_q x_q \right) \right\rangle = \sum_{n=1}^N P_n^2 \langle x_n^2 \rangle + 2 \sum_{k=1}^N \sum_{n=1}^{N-k} P_n P_{n+k} \langle x_n x_{n+k} \rangle \approx C_{x,0} \sum_{n=1}^N P_n^2 + 2 \sum_{k=1}^K C_{x,k} \left(\sum_{n=1}^N P_n P_{n+k} \right). \quad (11)$$

Mathematically, (11) is a sum of point-to-point products of the discrete correlation functions from both input pattern and the BLW pulse response. Factor 2 at the second sum means that summation should be done for positive and negative indices, which however were combined together due to symmetry. Upper index K in the second sum is a maximal correlation distance

between the symbols of the input pattern so that $C_{x,k} \approx 0$ for $k > K$. In many practical cases K is less than N , the length of the BLW pulse response in UI.

As we see from (11), it's enough to find K sums $\sum_{n=1}^N P_n P_{n+k}$ and multiply them on the pattern correlation coefficients, then add the result to dispersion of an uncorrelated pattern.

Having additional terms in (11) doesn't mean that the resulted BLW noise increases. Correlation between samples of the BLW pulse response is strong, and their products remain positive in a wide range. However, correlation coefficients of the input pattern could be negative. Let's consider NRZ 8b10b input pattern applied to the same channel.

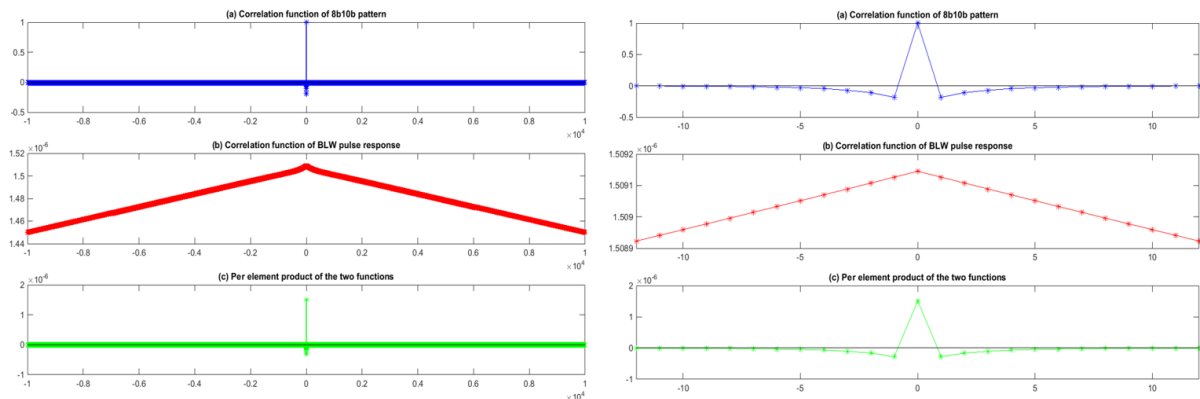


Figure 6. (a) Correlation function of 8b10b pattern, found from averaging over 10B symbols; (b) correlation function of BLW pulse response; (c) Their product, illustrating summands of (11)

In Figure 6, the right side is a zoomed version of the left. Correlation function of 8b10b, (a), was found by averaging the products $\langle x_n x_{n+k} \rangle$ over 10B symbols. Correlation length, however, is only a few symbols. Since 8b10b is DC balanced, the sum of the correlation coefficients is zero. Correlation function of BLW pulse response (b) changes very slowly and remains positive. By summing their sampled products we get $\sigma_y^2 = 1.7562e-10$ [V²], or BLW noise sigma equal 13.254 [uV]. This is about 2 orders of magnitude below the one for uncorrelated pattern.

BLW caused by periodic test pattern (PRBS-N and others)

BLW noise is often modeled by applying periodic test patterns [9], which is simpler than performing full time domain or statistical analysis. Here we show how to find the response to such input.

As shown above, we can find m -th state variable after N consecutive symbols using (6). However, our assumption was that all state variables were initially zero. Let's consider two cases.

If the period N of the test pattern is *shorter than the length of the BLW response*, we should first initialize state variables for any n -th symbol within a period as

$S_{m,n} = E_m^{N-1} x_{n-N+1} + E_m^{N-2} x_{n-N} + \dots + E_m x_{n-1} + x_n$. If the input pattern is N -periodic, state variables become cyclostationary. Then, the stationary values for the same symbol within a period become $z_{m,n} = S_{m,n} (1 + E_m^N + E_m^{2N} + E_m^{3N} \dots)$. Here, we used the fact that the contribution

from more distant periods is attenuated by an exponential multiplier $(E_m^N)^{K_p}$, where integer K_p shows how many periods ago they occurred. Recalling the sum of infinite geometric progression, we get $z_{m,n} = \frac{S_{m,n}}{1 - E_m^N}$. Once the state variables have been found for any symbol in a periodic pattern, there is no need to find partial sums for the other symbols. We can apply a recursive formula $z_{m,n} = E_m z_{m,n-1} + x_{n-1}$ and find all other values in a period. Then, the respective values of BLW noise are $y_n = \sum_{m=1}^M \text{Re}\{K_m z_{m,n}\}$.

Next, if the period of the input pattern *exceeds the length of BLW response*, we can truncate the summation when finding partial sum $S_{m,n}$. Also, there is no need in this case for cyclostationary correction. Then, we'll have to go through one full period with recursive update, possibly using aggregation of symbols together, as we did in time domain analysis.

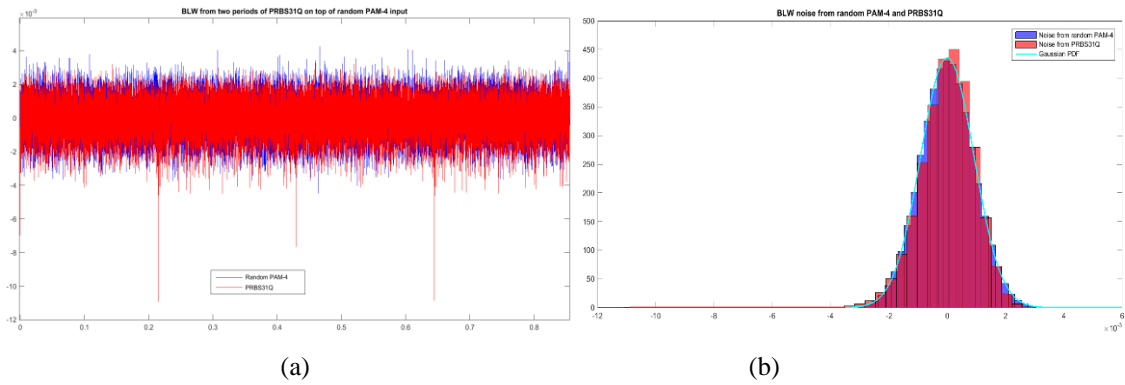


Figure 7. (a) BLW noise caused by two periods of PRBS31Q (red) on top of BLW noise from random PAM-4 pattern (blue); (b) almost Gaussian histogram from random PAM-4 pattern (blue) and asymmetrical from PRBS31Q (red)

We applied this method to find BLW noise caused by two periods of PRBS31Q pattern, for the same channel and symbol interval, about 4B symbols total. The waveforms are shown in Figure 7a. The response from PRBS31Q demonstrates abnormally larger undershoots, down to -10.93 mV. Random PAM-4 produces nearly Gaussian distribution, with $\sigma_x = 0.9153$ mV (Figure 7b). It is smaller than that found statistically for NRZ input by factor $\sqrt{5/9}$, which agrees with (10). The effects of ISI and BLW were computed with separate solvers working with different rates: BLW noise was updated once per 1K symbols using the “aggregated” input.

SER plot and its cross-sections found from 4B symbol time domain simulation is shown in Figure 8. The effect of BLW noise on the SER profile is consistent with its histogram in Figure 7. Note however that the BLW noise shown in Figure 7 is what we miss in the eye diagram when ignoring BLW. The BLW error has opposite polarity. That’s why large negative undershoots in Figure 7 make the eye shrink in the positive direction.

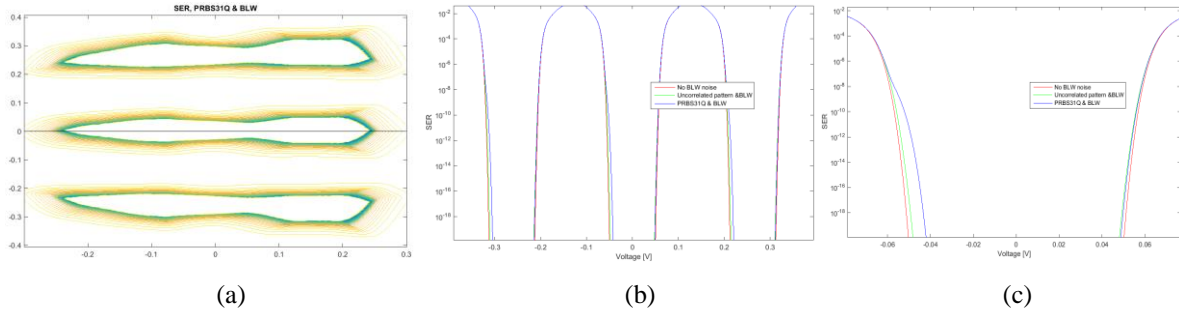


Figure 8. (a) SER built from PRBS31Q test pattern; (b) vertical cross-section of SER at $x_{UJ} = 0$ with uncorrelated input and BLW noise ignored (red), same with BLW considered (green), and with PRBS31Q and BLW noise considered (blue); (c) is the same zoomed around the central eye

X. Important factors affecting BLW noise

The value of DC blocking capacitor

By reducing the value of the DC blocking capacitor we increase BLW cutoff frequency, and hence, the power of the BLW noise. Both random uncorrelated and PRBS31Q patterns behave very similar to Figure 7a, but demonstrate larger magnitude. Figure 9 shows the peak values for random uncorrelated PAM-4 pattern and PRBS31Q. General trend agrees with

theoretical prediction ($\sim \frac{1}{\sqrt{C_{dc}}}$), shown by dashed green. However, there is a certain

deviation from this rule, especially for PRBS31Q. There are many reasons for that: BLW response is not exactly exponential, the pattern is not random uncorrelated and its LF spectrum may have low-frequency frequency resonances interacting with BLW response, etc.

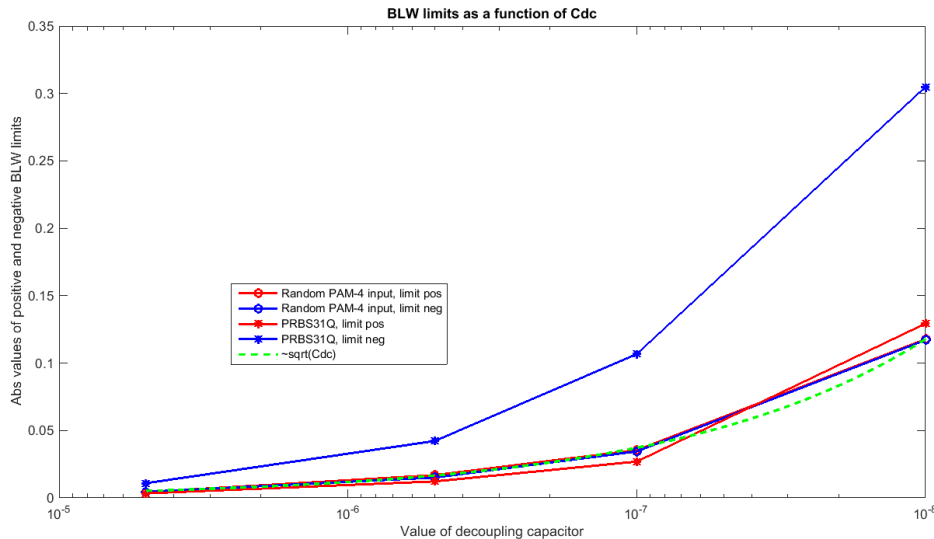


Figure 9. Peak values of BLW noise (red – positive, blue – negative) for random PAM-4 and PRBS31Q

Transmit jitter

Transmit jitter modifies symbol length and therefore modulates the average running imparity. For example, a DC balanced pattern affected by pulse interval modulation (PIM) may create considerable BLW noise. The effect is hard to predict because it depends on BLW transfer

function and two independent processes: input pattern and its pulse interval modulation caused by jitter. From a BLW perspective, random or deterministic jitter is especially harmful when correlated with averaged imparity of the pattern. The “averaging window” can be as small as one symbol or may be as long as the BLW response duration. Consider a simple clock pattern as an example: one percent of duty cycle distortion results in a systematic BLW component that is 2% of $A_s H_0$, or the signal level. Irregular patterns create a more complicated dependence of BLW noise on Tx jitter. Figure 9 illustrates the effect of duty cycle and sine jitter on BLW for PRBS31Q and random PAM-4 inputs. As we see, jitter may occasionally increase or decrease BLW noise over time.

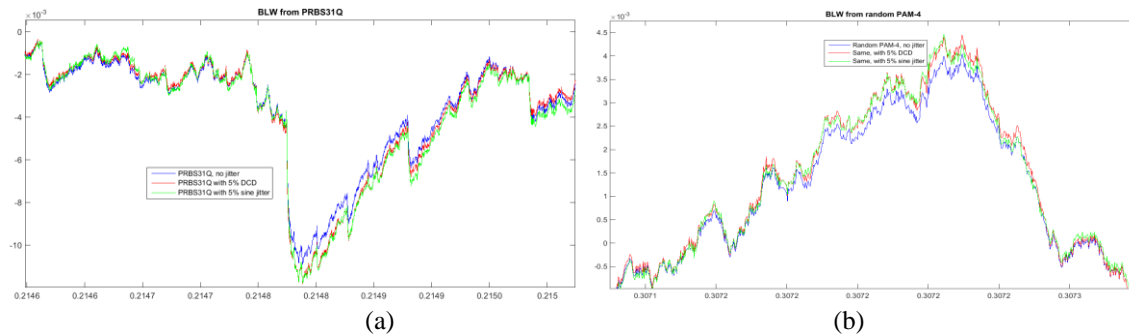


Figure 9. (a) BLW caused by PRBS31Q without jitter, with DCD and sine jitters; (b) same but for random uncorrelated PAM-4 pattern

Channel equalization

Linear equalization (FFE and CTLE) works in two different ways. On one hand, it reduces level separation by reducing signal transfer at low frequency. On the other, it lowers the BLW transfer function approximately in the same proportion. The sum effect on BLW-related error is not clear. Two other factors could be reducing ISI but increasing crosstalk. Non-linear equalization (DFE) appears neutral to BLW.

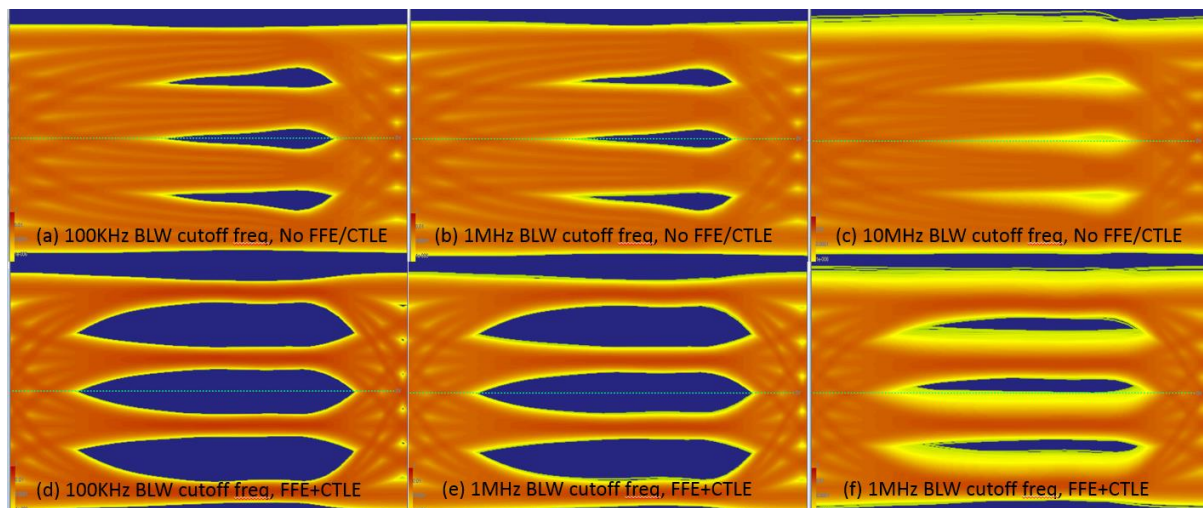


Figure 10. Top row (a-c): no equalization, while BLW cutoff frequency is 100kHz, 1MHz, and 10MHz. Bottom row (d-f): same as above by with identical FFE/CTLE equalization

We performed a series of simulations while increasing BLW cutoff frequency (hence, BLW noise), with and without linear equalization. As we see from Figure 10, the eye diagrams becomes progressively closed (left to right), due to BLW noise increase. Equalization

improves the eye, but doesn't cope with BLW noise. On the other hand, equalization doesn't increase BLW noise, as we see from comparing the two plots on the right.

XI. Correlations with measurement results

Experiment Design

The purpose of the measurements is to correlate the effects of BLW on the global performance of the PAM4 signaling from the point of view of the receiver. Effects of BLW are examined in the context of global attributes that qualify PAM4 signaling from the receiver angle.

The following industry standard qualifiers are assessed:

1. BER qualified eye openings, horizontal and vertical for all 3 PAM4 eyes.
2. Data Dependent Noise (DDN)
3. Signal levels
4. Level linearity of PAM4 signals
5. Eye closure penalty

Test Patterns

The ideal test pattern would be a PRBS31 that stresses most the BWL effects. The reality is that no acquisition system can acquire such long patterns with enough resolution, so instead the SSPRQ (Short Stress Pattern Random Quaternary) test pattern, with length set to PRBS16, $2^{16}-1$ precisely, is used. The SSPRQ is comprised of 4 segments, each based on key stressors from PRBS31. It is a stressful pattern, but short enough to allow for advanced analysis of jitter, noise, and BER with Equalization.

To compare results with less stressful patterns, measurements are performed with PRBS15 and PRBS13, which have the benefit of higher throughput acquisition, but effective in assessing the intersymbol interference due to limited bandwidth.

Data Source

In order to isolate the effects of BWL from bandwidth limitations of the target DUT, we chose to perform the measurements at 26.5625Gbaud, PAM4 data. The PAM4 pulse modulation was selected because of the critical loss of 9dB signal-to-noise ratio when moving from NRZ to PAM4.

The values of DC blocking capacitor

The acquisition and analysis was performed on a data stream that included a series of DC blocking capacitors between the signal generator and the front end of the acquisition module.

Testing was performed with:

- No DC blocking capacitor inserted

- 30nF, 220nF, 1uF capacitors inserted in the signal path.

Signal Source and Acquisition System

Signal source is a PAM4 pattern generator that provides all test pattern configurations.

The acquisition system is a 60GHz bandwidth remote head module.

Eye Measurements

The PAM4 Eye openings, horizontal and vertical are evaluated at the receiver slicer position, as specified by IEEE standard. Since PAM4 signaling is typically using Forward Error Correction (FEC), the target BER for these Eye measurements is $5e-5$.

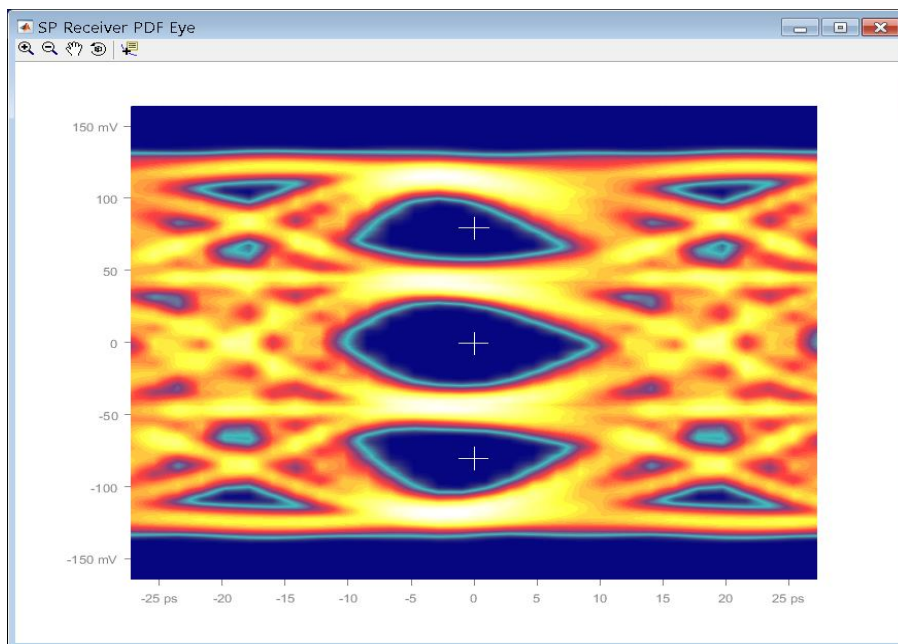
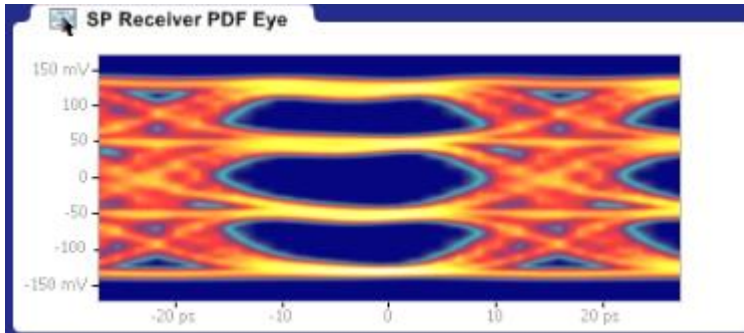


Figure 11 PDF Eye Modeling Receiver Slicer

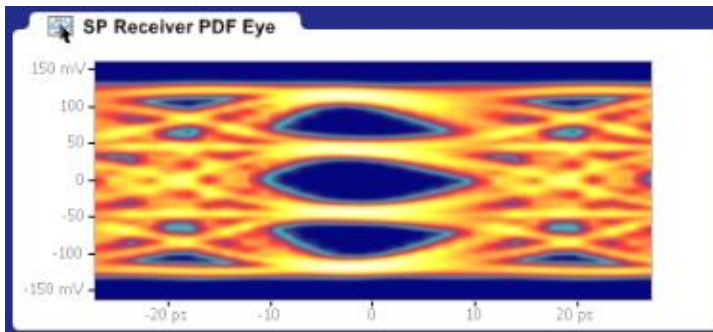
In following tables record the results of global jitter, noise and eye measurements for no blocking capacitor, and 3 different DC blocking capacitors.



Global Measurements	
Minimum Signal Level	38.64 mV
Effective Symbol Level 1	0.40
Effective Symbol Level 2	0.40
Level Mismatch (R_{LM})	0.89
Level Deviation	13.41%
Level Thickness	0.41%
Level Time Deviation	0.00%
Vertical Eye Closure	4.45 dB
VMA Outer	259 mV

BER = $5E-5$	RJ (RMS)	TJ	Eye Width	Decision Threshold	RN (RMS)	TN	Eye Height	Sampling Phase	Center Deviation	VMA
Eye2	518 fs	16.9 ps	20.7 ps	86.3 mV	642 uV	30.8 mV	46.0 mV	0 s	0 s	77.7
Eye1	519 fs	14.6 ps	23.1 ps	-87.9 uV	682 uV	27.5 mV	71.0 mV	0 s	0 s	104.7
Eye0	518 fs	18.7 ps	18.9 ps	-86.5 mV	624 uV	23.9 mV	55.4 mV	0 s	0 s	78.7

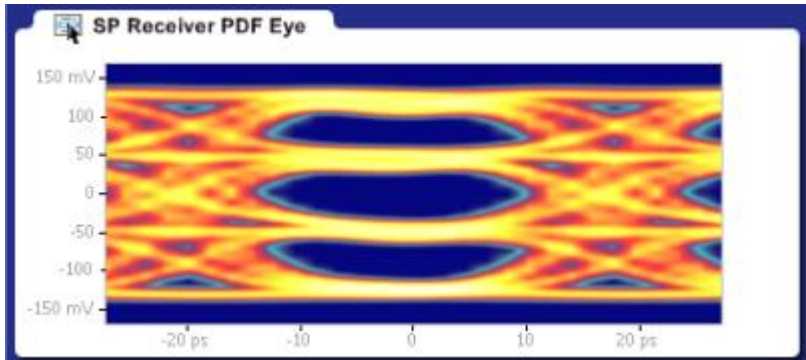
Figure 12 No DC blocking capacitor



Global Measurements	
Minimum Signal Level	37.37 mV
Effective Symbol Level 1	0.37
Effective Symbol Level 2	0.37
Level Mismatch (R_{LM})	0.94
Level Deviation	7.51%
Level Thickness	0.38%
Level Time Deviation	0.00%
Vertical Eye Closure	6.94 dB
VMA Outer	240 mV

BER = $5E-5$	RJ (RMS)	TJ	Eye Width	Decision Threshold	RN (RMS)	TN	Eye Height	Sampling Phase	Center Deviation	VMA
Eye2	481 fs	27.3 ps	10.3 ps	79.3 mV	502 uV	39.4 mV	32.2 mV	0 s	0 s	74.7 mV
Eye1	481 fs	18.7 ps	18.9 ps	-600 uV	520 uV	33.5 mV	51.7 mV	0 s	0 s	88.9 mV
Eye0	481 fs	26.0 ps	11.7 ps	-80.5 mV	486 uV	34.9 mV	37.3 mV	0 s	0 s	76.0 mV

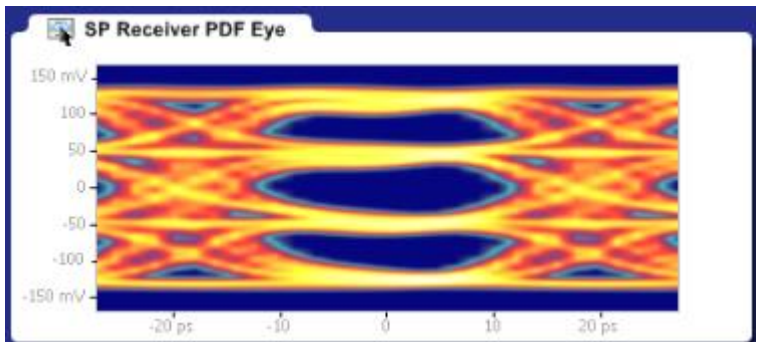
Figure 13 DC blocking capacitor – 30nF



Global Measurements	
Minimum Signal Level	38.12 mV
Effective Symbol Level 1	0.40
Effective Symbol Level 2	0.40
Level Mismatch (R_{LM})	0.90
Level Deviation	12.53%
Level Thickness	0.40%
Level Time Deviation	0.00%
Vertical Eye Closure	6.87 dB
VMA Outer	253 mV

BER = 5E-5	RJ (RMS)	TJ	Eye Width	Decision Threshold	RN (RMS)	TN	Eye Height	Sampling Phase	Center Deviation	VMA
Eye2	503 fs	19.7 ps	18.0 ps	83.9 mV	569 uV	40.2 mV	33.4 mV	0 s	0 s	76.5 mV
Eye1	503 fs	15.0 ps	22.7 ps	-360 uV	591 uV	37.4 mV	55.9 mV	0 s	0 s	100 mV
Eye0	503 fs	19.8 ps	17.8 ps	-84.7 mV	585 uV	33.4 mV	41.5 mV	0 s	0 s	76.2 mV

Figure 14 DC blocking capacitor – 220nF



Global Measurements	
Minimum Signal Level	38.60 mV
Effective Symbol Level 1	0.38
Effective Symbol Level 2	0.39
Level Mismatch (R_{LM})	0.90
Level Deviation	10.78%
Level Thickness	0.40%
Level Time Deviation	0.00%
Vertical Eye Closure	7.12 dB

BER = 5E-5	RJ (RMS)	TJ	Eye Width	Decision Threshold	RN (RMS)	TN	Eye Height	Sampling Phase	Center Deviation	VMA
Eye2	527 fs	18.0 ps	19.7 ps	84.3 mV	572 uV	41.4 mV	32.6 mV	0 s	0 s	77.2 mV
Eye1	528 fs	15.3 ps	22.3 ps	-1.08 mV	607 uV	39.4 mV	54.4 mV	0 s	0 s	99.2 mV
Eye0	527 fs	19.6 ps	18.1 ps	-86.5 mV	574 uV	35.1 mV	40.1 mV	0 s	0 s	79.8 mV

Figure 15 DC blocking capacitor – 1uF

By inserting a 3nF capacitor the horizontal and vertical eye openings at 5e-5 BER drop as much as by a factor of 2.

Total Noise increases due to BLW from about 30mV to 39mV for the top PAM4 eye. The plot below is a validation of the plot in figure 9, showing noise increase in function of DC

block capacitor value. This is a reverse, showing the Vertical Eye opening in function of the DC block value.

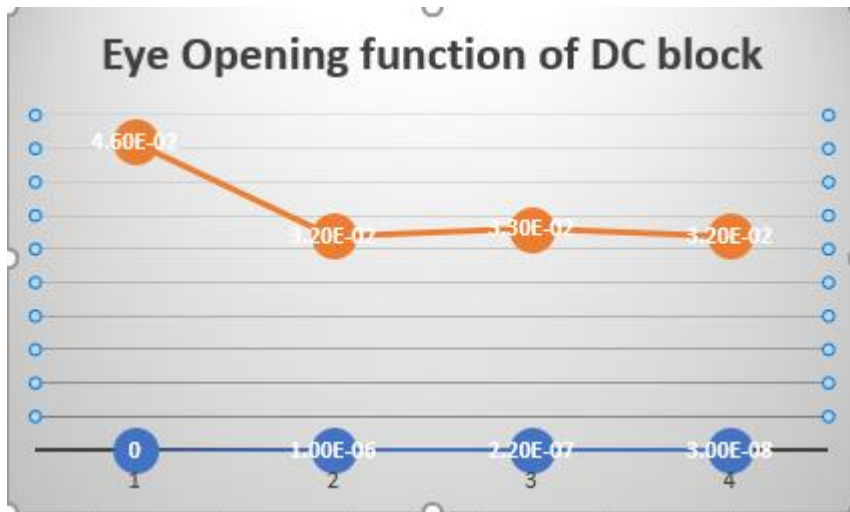


Figure 16 Vertical Eye opening function of DC block.

A deeper look into the noise analysis for the acquired data, shows clearly that, as expected, the contribution to the increase of Total Noise is due to the Data Dependent Noise, which points to the BLW as the cause for the increase of the deterministic noise.

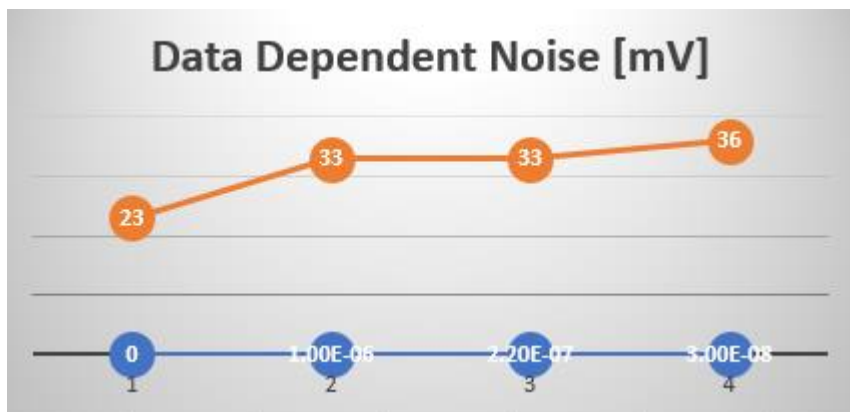


Figure 17 Data Dependent Noise function of DC block.

Global PAM4 measurements: Linearity Mismatch, Vertical Eye Closure, Level Deviations

IEEE and OIF Standards have defined a number of global PAM4 measurements to assess the distortion of different sources, and that drive the overall BER performance of a serial link.

The question to answer is which of these measurements are affected by the BLW.

The Level Mismatch is a measure of the linearity, defined as the level deviation from an ideal level distribution. Ideal value for Level Mismatch Ratio is 1. As shown below, and as expected, the DC coupling capacitor does not affect the level symmetry.



Figure 18 Level Mismatch ratio function of DC block.

A third measurement to consider is Vertical Eye Closure penalty (VECP). Similar with the TDECQ (Transmitter and Dispersion Eye Closure Quaternary) used by the optical system, VECP identifies the smaller eye opening relative to an ideal given a signal amplitude. Ideal value is ~5dB for 3 equal PAM4 eyes. Correlating with the increase in the noise due to BLW, VECP will penalize the receiver.

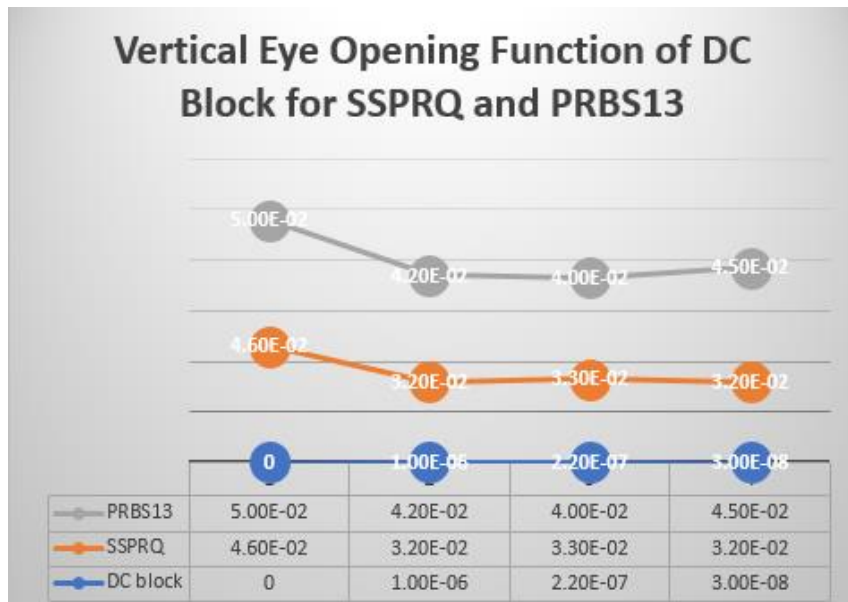


Figure 19 Vertical Eye Closure Penalty function of DC block.

Relevance of Test Patterns

In order to isolate the effects of Baseline Wander from effects of Intersymbol Interference and the effects of uncorrelated jitter and noise impairments, the testing was performed by using a series of standard PRBS patterns along the testing with the SSPRQ pattern.

The relevance of using the long runs for each symbol level is illustrated in figure 20, which shows the vertical eye measurement results function of DC block for SSPRQ and PRBS13. While SSPRQ was designed for compliance testing for optical links, it proves to be the required test pattern for isolating the effects of BLW.



XII. Conclusion

In this paper we considered Baseline Wander, an important impairment that should be considered in SERDES design process. We analyzed the cause of BLW, its difference from ISI, and proposed its analysis by using two independent characteristics of a channel, at low and high frequency. This can also be performed using two step responses which cover different time regions and complement each other. A separate low-frequency BLW characterization allows its fast and accurate analysis, both in time and statistical domains. We considered a number of input pattern types: random uncorrelated, non-deterministic and correlated with known correlation function, and deterministic periodic.

With multi-level modulation, and tighter signal margins in state of the art designs, BLW can no longer be ignored. We believe that the methods proposed in this paper would benefit different simulation and measurement approaches, including StatEye-type, IBIS-AMI, COM/PCIE/USB/JCOM compliance methodology, as well as BLW measurement techniques.

References

- [1] IEEE Standard for Ethernet, IEEE Std. 802.3bj-2014, Annex 93A
- [2] A. P. Clark, "Principles of digital data transmission", Willey, 1983
- [3] S. Haykin, "Digital communications", John Wiley & Sons, 1988
- [4] J. Proakis, "Digital communications", 4th edition, McGraw-Hill, 2000
- [5] F. Waldhauer, "Quantized feedback in an experimental 280 Mb/s digital repeater for coaxial transmission", IEEE Trans. on Communication, v.22, Jan. 1974
- [6] N. Sommer, L. Lusky, M. Miller, "Analysis of the probability distribution of the baseline wander effect for baseband PAM transmission with application to gigabit Ethernet", Proc. of the 2004 11th IEEE International Conference on Electronics, Circuits and Systems, ICECS 2004.

- [7] N. Na, D. Dreps, J. Hejase, "DC wander effect of DC blocking capacitors on PCI Gen3 signal integrity", 2013 IEEE 63rd Electronic Components and Technology Conference.
- [8] P. Anslow, "Baseline wander with FEC", IEEE P802.3bs Task Force, 2017
- [9] P. Anslow, "SSPRQ test pattern", IEEE P802.3bs Task Force, 2016
- [10] B. Gustavsen, A. Semlyen, "Rational approximation of frequency domain responses by vector fitting", IEEE Trans. Power Delivery, 1999, vol. 14
- [11] B. Gustavsen, C. Heitz, "Modal vector fitting: a tool for generating rational models of high accuracy with arbitrary terminal conditions", IEEE Trans. Adv. Packag., 2008, vol. 31
- [12] V. Dmitriev-Zdorov, V. Heyfitch, G. Pratt, "Fast time-domain simulation of 200+ port S-parameter models", DesignCon 2006.